International Journal of Pharmaceutics 643 (2023) 123216

Contents lists available at ScienceDirect

International Journal of Pharmaceutics

journal homepage: www.elsevier.com/locate/ijpharm

Zein-based nanospheres and nanocapsules for the encapsulation and oral delivery of quercetin

Raquel Campión [a], Carlos J. Gonzalez-Navarro [b], Ana Luisa Martínez López [a], M. Cristina Martínez-Oharriz [c], Cristina Matías [d], María-José Sáiz-Abajo [d], Maria Collantes [e,g], Ivan Peñuelas [e,f,g], Juan M. Irache [a,g,*]

[a] NANO-VAC Research Group, Department of Chemistry and Pharmaceutical Technology, School of Pharmacy and Nutrition, University of Navarra, 31008 Pamplona, Spain
[b] Center for Nutrition Research, School of Pharmacy and Nutrition, University of Navarra, 31008 Pamplona, Spain
[c] Department of Chemistry, University of Navarra, Pamplona, Spain
[d] National Centre for Food Technology and Safety (CNTA), NA 134, Km. 53. 31570-San Adrián, Navarre, Spain
[e] Radiopharmacy Unit, Clinica Universidad de Navarra, 31008 Pamplona, Spain
[f] Translational Molecular Imaging Unit (UNIMTRA), Department of Nuclear Medicine, Clinica Universidad de Navarra, 31008 Pamplona, Spain
[g] Institute for Health Research (IdiSNA), 31008 Pamplona, Spain

ARTICLE INFO

Keywords:
Nanospheres
Nanocapsules
Zein
Quercetin
Antihyperlipidemic effect
Bioavailability

ABSTRACT

In this study, the ability of zein nanospheres (NS) and zein nanocapsules containing wheat germ oil (NC) to enhance the bioavailability and efficacy of quercetin was evaluated. Both types of nanocarriers had similar physico-chemical properties, including size (between 230 and 250 nm), spherical shape, negative zeta potential, and surface hydrophobicity. However, NS displayed a higher ability than NC to interact with the intestinal epithelium, as evidenced by an oral biodistribution study in rats. Moreover, both types of nanocarriers offered similar loading efficiencies and release profiles in simulated fluids. In *C. elegans*, the encapsulation of quercetin in nanospheres (Q-NS) was found to be two twice more effective than the free form of quercetin in reducing lipid accumulation. For nanocapsules, the presence of wheat germ oil significantly increased the storage of lipids in *C. elegans*; although the incorporation of quercetin (Q-NC) significantly counteracted the presence of the oil. Finally, nanoparticles improved the oral absorption of quercetin in Wistar rats, offering a relative oral bioavailability of 26% and 57% for Q-NS and Q-NC, respectively, compared to a 5% for the control formulation. Overall, the study suggests that zein nanocarriers, particularly nanospheres, could be useful in improving the bioavailability and efficacy of quercetin.

1. Introduction

Quercetin (3,3′,4′,5,7-pentahydroxyflavone) is a dietary flavonoid present in some fruits and vegetables, such as tomato, lettuce, onion, black chokeberry, or apples (Luca et al., 2020). In fruits and vegetables, quercetin appears as quercetin glycoside, in which the aglycone is bound to sugar moieties, such as rutin and quercetrin (quercetin esterified with rutinose and rhamnose, respectively), being the first the most common and important glycoside form found in plants (Nabavi et al., 2015). The diet daily intake of quercetin varies greatly depending on the country and the diet followed. Using food consumption data from the European Food Safety Authority (EFSA) and the FLAVIOLA Food Composition Database, the daily intake in the EU would be between 9 and 21 mg quercetin per day (Vogiatzoglou et al., 2015). In other interesting studies, quercetin intake would be about 18 mg/day for Chinese healthy young males, whereas in US adults, the average intake would be of about 10 mg/day (Li et al., 2016).

A number of studies have shown that quercetin has multiple biological activities, including anti-inflammatory (Li et al., 2016), antihypertensive (Serban et al., 2016), antihyperglycemic (Dhanya, 2022) or antihyperlipidemic properties (Abdel-Raouf et al., 2011). Thus, quercetin would reduce the levels of triglycerides, total cholesterol, serum low-density lipoprotein cholesterol (LDL-C), and increased serum high-density lipoprotein cholesterol (HDL-C) in hyperlipidemic animals

* Corresponding author at: Dept. Chemistry and Pharmaceutical Technology, University of Navarra, C/ Irunlarrea, 1, 31008 Pamplona, Spain.
E-mail address: jmirache@unav.es (J.M. Irache).

https://doi.org/10.1016/j.ijpharm.2023.123216
Received 5 May 2023; Received in revised form 5 July 2023; Accepted 7 July 2023
Available online 8 July 2023

(Braun et al., 2017; Shao et al., 2016). This antihyperlipidemic effect of quercetin would be related to a specific inhibition of the intestinal absorption of cholesterol mediated by the epithelial cholesterol transporter Niemann-Pick C1-like 1 (NPC1L1) (Nekohashi et al., 2014). However, other mechanisms that may be involved would be the capacity of quercetin to reduce oxidative stress (Yang et al., 2019) and/or the up-regulation of some genes related to lipid metabolism (Mzhel'skaya et al., 2019). In humans, the lipid-lowering potential of quercetin have been evidenced with the oral administration of dietary supplements at daily doses higher than 400 mg/day and for at least 10 days (Mazza et al., 2021; Nishimura et al., 2019).

However, the oral bioavailability of quercetin remains a challenge. In fact, the aglycone shows a very poor aqueous solubility and it suffers for an extensive metabolism in the gastrointestinal tract. As consequence, the oral bioavailability is quite low (below 10%) (Kandemir et al., 2022). In the last years, different attempts and formulation strategies have been evaluated in order to improve quercetin absorption and bioavailability, including the use of complex with cyclodextrins (Başaran et al., 2022), micelles (Lu et al., 2018), nanoemulsions (Mahadev et al., 2022), or nanoparticles (Barbosa et al., 2019). In some cases, good oral bioavailability results have been obtained by including pharmaceutical excipients with inhibitory properties of esterases and/or intestinal P-gp (i.e., hydroxypropil-β-cyclodextrin (Peñalva et al., 2019), sodium oleate (Li et al., 2021) or Cremophor (Tran et al., 2014)) in the formulation of nanoemulsions or nanoparticles. Another interesting strategy has been the use of zein nanoparticles as oral carriers to improve the oral bioavailability of quercetin (Moreno et al., 2017; Penalva et al., 2017; Yang et al., 2022). Zein, the major storage protein of corn, is a prolamin insoluble in water with a GRAS (Generally Recognized as Safe) status. This protein has been proposed as excipient for the preparation of swelling matrix formulations (Bouman et al., 2015), and colonic delivery systems (Amidon et al., 2015), or film-coating agent for dragées (Winters and Deardorff, 1958) and tablets (Yin et al., 2015). Moreover, zein can be easily transformed into nanoparticles by different techniques, including electrospinning and desolvation based methods (Martínez-López et al., 2020).

Caenorhabditis elegans (*C. elegans*) is a powerful model for studying the effects and mechanisms of bioactive compounds, as polyphenols (Aranaz et al., 2020), as it harbours regulatory pathways highly conserved with mammals, including glucose homeostasis. As a result, under high glucose conditions, the worm shows shorter lifespan, increased oxidative stress and fat accumulation, mimicking changes observed in metabolic syndrome in mammals, and thus becoming a useful and cost-effective model for studying the effect of drugs or nutraceuticals (Kaletta and Hengartner, 2006; Zhu et al., 2016). Moreover, *C. elegans* is being used for initial screening of drugs delivery through nanocarriers, as it also shows similarities to the mammalian intestinal barrier, including transport of biomolecules, the presence of tight junctions and efflux pumps such as P-glycoproteins (Martínez-López et al., 2021).

The aim of this work was to gain insight in the capability of zein nanoparticles to promote the oral bioavailability of quercetin and its antihyperlipidemic effect. For this general purpose, two different zein-based nanoparticles were evaluated: zein nanospheres (NS) and zein nanocapsules (NC). The main difference between both nanocarriers was the presence of wheat germ oil in NC. This oil was selected because of its good solvent properties for quercetin.

2. Materials and methods

2.1. Materials

Quercetin, zein, L-lysine, 2-hydroxypropyl-β-cyclodextrin (HP-β-CD), trifluoroacetic acid, Rose Bengal, sodium chloride, dipotassium hydrogen phosphate, magnesium chloride, sodium phosphate dibasic heptahydrate, Orlistat, glucose, sterile DMSO, Nile Red, Kollisolv® PEG 400, and sulfadimetoxine were purchased from Sigma-Aldrich (Saint Louis, MO, USA). Wheat germ oil and mannitol were obtained from Guinama (La Pobla de Vallbona, Spain). Absolute ethanol and isopropanol were from Scharlab (Sentmenat, Spain). Acetonitrile (ACN, HPLC grade), methanol (HPLC grade), calcium chloride, and EMPLURA® Sodium hypochlorite solution (6–14% active chlorine) were purchased from Merck (Darmstadt, Germany). Lumogen® Red 305 was provided by BASF (Ludwigshafen am Rhein, Germany). Hydrochloric acid 37%, formaldehyde 3.7–4.0 % w/v buffered to pH = 7 and stabilized with methanol, and UHPLC grade ACN were acquired from Panreac AppliChem (Castellar del Vallès, Spain). Phosphate Buffered Saline (PBS) was obtained from Gibco (Thermo Fisher Scientific, Waltham, MA, USA). Magnesium sulphate heptahydrate and formic acid were purchased from VWR Chemicals (Radnor, PA, USA). Potassium phosphate monobasic was from Acofarma (Madrid, Spain), and sodium hydroxide from Honeywell (Charlotte, NC, USA). European bacteriological agar, peptone, LB Broth, and agarose were provided by Condalab (Torrejón de Ardoz, Spain). Isoflurane (IsoVet®) was acquired from B. Braun Vetcare (Rubí, Spain). Tissue-Tek® O.C.T. Compound was purchased from Sakura Finetek Europe (Alphen aan den Rijn, The Netherlands), and commercial rat plasma was obtained from Envigo (Indianapolis, IN, USA).

2.2. Preparation of nanoparticles

2.2.1. Zein nanospheres (NS)

Zein nanospheres (empty or loaded with quercetin) were prepared by a previously reported desolvation method with some modifications (Penalva et al., 2017). Thus, 200 mg zein and 30 mg L-lysine were mixed in 20 mL of a hydroalcoholic solution (ethanol 70% v/v) with magnetic stirring and nanospheres were formed by the slow addition of 20 mL purified water. Then, 2 mL of an aqueous solution of mannitol (200 mg/mL) were added and the suspensions were dried in a mini Spray Dryer B-290 (Büchi Labortechnik AG, Flawil, Switzerland). Quercetin-loaded nanospheres (Q-NS) were prepared and dried, in the absence of mannitol, as described above after the addition of 20 mg quercetin in the initial hydroalcoholic solution of zein and lysine.

2.2.2. Zein nanocapsules (NC)

NC were obtained in a similar way as described for the preparation of nanospheres, with the difference of the incorporation of an oily compound. Briefly, 200 mg zein and 30 mg L-lysine were mixed in 17 mL of a hydroalcoholic solution (ethanol 65% v/v) with magnetic stirring. In parallel, 22 μL of wheat germ oil were dissolved in 3 mL ethanol and added to the initial solution of zein and lysine. Then, 20 mL water were added to induce the formation of the nanocapsules. Finally, after the addition of a solution of mannitol (400 mg in 2 mL water), nanocapsules were dried in the mini Spray Dryer B-290. For the preparation of quercetin-loaded nanocapsules (Q-NC), 20 mg quercetin were added to the initial mixture of zein, oil, and lysine before the formation of nanocapsules. Then, the nanocapsules were dried, in the absence of mannitol, as described above.

2.2.3. Lumogen® Red-loaded nanoparticles

Lumogen® Red was loaded in zein nanospheres and nanocapsules. For this purpose, 2.7 mL of a solution of Lumogen® Red in ethanol was added to the initial mixture of zein, oil and lysine, before the addition of water to form the nanoparticles. The resulting nanodispersions were dried, in the absence of mannitol, as described above.

2.2.4. Technetium-labelled nanoparticles (^{99m}Tc-nanoparticles)

The radiolabelling was performed in a direct way by reduction and reaction of a solution of technetium-99 m (^{99m}Tc) with the nanoparticles. For that purpose, 2.5 mg nanoparticles were dispersed in 100 μL water, and 50 μL of a solution of $SnCl_2{\cdot}2H_2O$ (0.05 mg/mL) were added, purging afterwards the dispersion with N_2 for 5 min. Then, 111

± 11 MBq of a solution of [^{99m}Tc]TcO_4^- was added, obtained from a ^{99}Mo/^{99m}Tc generator (8,6 GBq Drytec, General Electric, Boston, MA, USA), in a volume lower than 200 μL. After incubation for 10 min, the radiolabelling was verified by radio-TLC, using iTLC-SG paper (Agilent Technologies, Santa Clara, CA, USA) as stationary phase and 2-butanone as mobile phase, where ^{99m}Tc-nanoparticles remain in the origin and free [^{99m}Tc]TcO_4^- moved forward. Finally, the sample was mixed with 7.5 mg of non-modified nanoparticles.

2.3. Characterization of nanoparticles

2.3.1. Size, zeta potential and morphology

The size and zeta potential of the nanoparticles was measured in a ZetaPlus Analyzer (Brookhaven Instrument Corporation, Holtsville, NY, USA), by dynamic light scattering (DLS) and electrophoretic light scattering (ELS), using a dispersion of the formulations in water. The content of zein in the nanoparticles was quantified using a MicroBCA Protein Assay Kit (Thermo Fisher Scientific, Waltham, MA, USA), following the instructions of the manufacturer.

The morphology of nanoparticles was analyzed by scanning electron microscopy (SEM) in a FE-SEM Sigma 500 (Zeiss Microscopy, Jena, Germany). For the preparation of the samples, mannitol-free nanoparticles were redispersed in 1 mL water before mounted in SEM grids and coated with a gold layer using an Emitech K550 sputter coater (Quorum Technologies, Laughton, UK).

2.3.2. Fourier Transform infrared spectroscopy (FTIR) analysis

Dry powder of nanoparticles was placed in the diamond crystal of a Fourier Transform spectrophotometer IR Affinity-1S (Shimadzu, Kyoto, Japan) equipped with a MKII Golden-Gate single reflection ATR system (Specac, Orpington, UK), and spectra were collected from 600 to 4,000 cm^{-1} with a resolution of 2 cm^{-1} and 50 scans per spectrum. Data were then analyzed with Labsolution IR software (Shimadzu, Kyoto, Japan).

2.3.3. Hydrophobicity assay

The hydrophobicity of the nanoparticles was analyzed using the Rose Bengal method previously described (Reboredo et al., 2021). Briefly, samples of nanoparticles were incubated with an aqueous solution of Rose Bengal (100 μg/mL) before centrifugation 30 min (13500 g at 4 °C) in a Mikro 220R Hettich centrifuge (Hettich, Tuttlingen, Germany). Then the absorbance of supernatants was measured at 548 nm in a BioTek PowerWave XS microplate spectrophotometer (BioTek Instruments Inc, Winooski, VT, USA).

2.3.4. Diffusion of nanoparticles in pig intestinal mucus by multiple particle tracking (MPT)

Fluorescently labelled nanoparticles with Lumogen® Red were used to analyse the diffusion of nanoparticles through pig intestinal mucus, based on the multiple particle tracking technique (Abdulkarim et al., 2015). For this purpose, 4 mg of formulation powder were dispersed in 1 mL water, and 25 μL of this suspension was incorporated in approximately 0.5 mL pig intestinal mucus. The sample was incubated for 2 h in a Labnet Vortemp 56 EVC incubator (Labnet International Inc., Edison, NJ, USA) at 37 °C and 300 rpm before visualization in a Confocal Microscope Cell Observer Z1 (Zeiss Microscopy, Jena, Germany) equipped with a Plan-Apochromat 63x/1.4 Oil objective and using the rhodamine filter. Videos of 15 s and a total of 378 frames were captured and analyzed using Fiji ImageJ. The diffusion coefficient of the nanoparticles in water (D°) was estimated by the Stokes-Einstein equation (Reboredo et al., 2021), whereas the "Effective Diffusion Coefficient" (<Deff >) was calculated as follows:

$$< Deff >= \frac{< MSD >}{4 \bullet \Delta t} \quad (1)$$

in which < MSD > is the mean square displacement of 100 trajectories and *4* is a constant related to the 2-dimensional mode of video capture.

The diffusion of the particles was also expressed as the ratio < Deff>/ D° (%).

2.3.5. Quercetin content

The payload of quercetin in the nanoparticles was quantified in an Agilent 1200 Series HPLC System with an UV–Vis detector (Agilent Technologies, Santa Clara, CA, USA), using a Kinetex C18 column (5 μm, 100 Å, 100 × 4.6 mm) and a C18 SecurityGuard™ ULTRA Cartridge precolumn for 4.6 mm ID columns (Phenomenex, Torrance, CA, USA). An isocratic mobile phase of 0.1% trifluoroacetic acid (TFA) in water and 0.1% TFA in acetonitrile (ACN) (60:40) was used, with a flow rate of 0.7 mL/min, an injection volume of 10 μL, and a column temperature of 40 °C. Quercetin was detected at a wavelength of 370 nm, and the retention time (RT) was 2.3 min. Calibration curves were prepared from 2 to 100 μg/mL in ethanol ($R^2 \geq 0.9997$). The limit of detection was calculated to be 0.5 μg/mL and the limit of quantification was 1.6 μg/mL.

For the preparation of the samples, 5 mg of each formulation were dissolved in ethanol 75% (v/v) and vortexed for 1.5 min to break the nanoparticles. A dilution with absolute ethanol (0.4 mL to 2 mL) was made before injecting the samples in the chromatograph. Samples were prepared in triplicate and data were expressed as μg of quercetin loaded by milligram nanoparticles. The encapsulation efficiency (expressed in percentage) was calculated as the quotient between the payload of quercetin in the nanoparticles and the quantity initially added.

2.4. In vitro release studies

In vitro release studies of quercetin from nanoparticles were carried out in simulated gastric (SGF, pH 1.2) and intestinal fluids (SIF, pH 6.8) containing 1% (w/v) of 2-hydroxypropyl-β-cyclodextrin (HP-β-CD) as a solubilizing agent in order to offer sink conditions. Experiments were carried out at 37 °C in an Unitronic 320 OR bath (P Selecta, Barcelona, Spain) with stirring (300 rpm) using a Cimarec™ i Telesystem Multipoint Stirrer (Thermo Fisher Scientific, Waltham, MA, USA). Thus, amount of nanoparticles equivalent to 250–300 μg quercetin (12.1 mg of each formulation approximately) was dispersed in 5 mL water and introduced in a Float-A-Lyzer®G2 Dialysis Device with a molecular weight cut-off of 300 kD (Spectrum Laboratories, Inc., Rancho Dominguez, CA, USA). Immediately, the devices were immersed in 47 mL of SGF and after 2 h, changed to 47 mL of SIF. At different time points, 500 μL of external media was taken, replacing the extracted volume with new media, and immediately analyzed by HPLC. Quercetin was quantified using the chromatographic method previously described. In this case, calibration curves were prepared in ethanol ranging from 0.3 μg/mL to 12 μg/mL ($R^2 \geq 0.998$). The limit of detection was calculated to be 0.3 μg/mL and the limit of quantification 0.9 μg/mL.

2.5. Biodistribution of nanoparticles within the gut

In order to evaluate the biodistribution in vivo, nanoparticles were labelled with either ^{99m}Tc or with Lumogen® Red. In the former, radiolabeling ^{99m}Tc-nanoparticles were employed to gain insight about their gastro-intestinal transit, whereas fluorescently labelled nanoparticles were employed to evaluate their biodistribution at the microscopical level. Experiments were approved by the Ethical and Biosafety Committee for Research on Animals of the University of Navarra (protocol number 066–16 and 045–18).

For radiolabeled ^{99m}Tc-nanoparticles, animals (approx. 250 g; Envigo, IN, USA) were slightly anesthetized with 2% isoflurane gas before receiving by gavage 1 mL of nanoparticles in water. Animals were scanned by single photon emission computed tomography (SPECT) in a U-SPECT6/E-class (MILabs, Houten, The Netherlands) using a UHR-RM-1 mm multi-pinhole collimator. After 4 h of the administration, rats were

placed prone on the scanner bed under continuous anesthesia with isoflurane (2% in 100% O_2 gas) to acquire a whole-body scan over 15 min. Following the SPECT acquisition, CT scans were performed to obtain anatomical information using a tube setting of 55 kV and 0.33 mA. The SPECT images were reconstructed using the ^{99m}Tc photopeak centered at 140 keV with a 20% energy window width and using a calibration factor to obtain the activity information (MBq/mL). Finally, attenuation correction was applied using the CT attenuation map. Studies were visualized using PMOD software (PMOD Technologies Ltd., Adliswil, Switzerland).

For nanoparticles fluorescently labelled with Lumogen® Red, the animals also received orally 1 mL of either NS or NC dispersed in water (approx. 10 mg). After 4 h post-administration, animals were sacrificed and different parts of the gastrointestinal tract were extracted (portions of around 1 cm), washed with PBS, collected in Tissue-Tek® O.C.T. and frozen at −80 °C until analysis. The samples were sliced, fixed with formaldehyde and washed before treatment with DAPI (2.5 μg/mL) for 15 min (Inchaurraga et al., 2015). Pictures were taken in an Automated Microscope Zeiss Axio Imager M1 with an Axiocam MRm camera (Zeiss Microscopy, Jena, Germany) using the DAPI filter.

2.6. In vivo studies in Caenorhabditis elegans

2.6.1. C. Elegans strains and maintenance

Wild-type N2 Bristol strain was obtained from the *Caenorhabditis Genetics Center* (CGC, University of Minnesota, MN, USA) and grown in Nematode Growth Medium (NGM) at 20 °C, using *Escherichia coli* OP50 as normal diet. For the following experiments, the nematodes were age-synchronized by standard sodium hypochlorite treatment. Finally, eggs were incubated in M9 medium for at least 18 h to promote the hatching.

2.6.2. Intake of nanoparticles

To evaluate the ingestion of nanoparticles by the worms, L1/L2 larvae were grown to L4 larvae in NGM. Treatment plates were prepared as a mixture of NGM and Lumogen® Red-loaded nanospheres, adding *E. coli* on the surface of the dry media. At L4 stage, worms were put in these plates and two hours later, they were collected with PBST (0.01% Triton X-100 in Phosphate Buffered Saline) and placed in a 2% agarose pad with 1% of sodium azide (w/v). Samples were visualized using an Automated Microscope Zeiss Axio Imager M1 with an Axiocam MRm camera (Zeiss Microscopy, Jena, Germany), using the rhodamine filter to visualize the Lumogen® Red-loaded nanospheres and the DAPI filter to see the autofluorescence of the worms. The photographs were taken with ZEN software (Zeiss Microscopy, Jena, Germany) and processed with ImageJ.

2.6.3. Evaluation of fat accumulation

The evaluation of the accumulation of fat in the body of the nematode *C. elegans* was performed by the Nile Red method, as previously described (Navarro-Herrera et al., 2018; Martinez-Lopez et al., 2021). For this purpose, glucose-supplemented NGM (0.5% w/v glucose) was used to evaluate the effect of the nanoencapsulated quercetin on the accumulation of fat, at a concentration equivalent to 50 μM quercetin. Orlistat was used as a positive control of fat reduction (6 μg/mL in DMSO). Once the plates were prepared, dried, and *E. coli* was added, between 300 and 500 L1/L2 larvae per well were transferred. After 46 h, L4 worms were collected in 1 mL PBST for each well, centrifuged for 4 min at 263 g in a Microfuge® 16 centrifuge (Beckman coulter, Brea, CA, USA), and the supernatant was eliminated. Worms were redispersed in PBST and put in ice for 15 min before eliminating supernatants. Then, 200 μL isopropanol 40% (v/v) were added to the pellet and, after 3 min of incubation, the samples were centrifuged. The supernatant was eliminated, 150 μL of Nile Red staining (3 μg/mL in isopropanol 40% vol.) was added, and the mixture was incubated at 20 °C for 25–30 min in an orbital shaker at 60 rpm. Then, samples were centrifuged, the supernatant was again removed, and the obtained pellet was washed with 1 mL PBST. Finally, the pellet containing the worms were mounted in a 2% agarose pad and visualized in a fluorescent microscope. Images were taken at 100x magnification in a Nikon SMZ18 stereomicroscope equipped with an epi-fluorescence system with a DS-FI1C refrigerated color digital camera (Nikon Instruments Inc., Tokyo, Japan), using a GFP filter (Ex 480–500; DM 505; BA 535–550), and fat was quantified using the software ImageJ.

2.7. Pharmacokinetic study

For the pharmacokinetic assay, Wistar rats were purchased from Envigo (Indianapolis, IN, USA) and acclimated at least for a week, in 12 h dark/light cycles at 23 ± 2 °C, with free access to food and water. All the experiments were approved by the Ethical and Biosafety Committee for Research on Animals of the University of Navarra (protocol number 056–19).

Rats were fasted overnight and an oral single dose of quercetin (15 mg/kg), either as an aqueous formulation (Q) or loaded in nanoparticles dispersed in water, was administered by oral gavage. Q was prepared by incorporating 6.25 mg/mL quercetin and 30.2 mg/mL HP-β-CD in purified water (Penalva et al., 2017). At different times, animals were anesthetized with inhaled isoflurane and blood samples were extracted from the tail vein and added to EDTA tubes. As intravenous control, a solution of quercetin in a mixture of PEG 400 and water for injection (6:4 by vol.) was employed (Penalva et al., 2017). All blood samples were centrifuged for 10 min at 2,500 g and 4 °C, and supernatants were collected and frozen at −80 °C for further quantification.

For quercetin extraction, 100 μL of each plasma sample was mixed with 600 μL of cold 0.95% (v/v) HCl in methanol. Samples were vortexed at 2,500 rpm in a DXV-2500 Multi-Tube Vortexer (VWR International, Radnor, PA, USA) for 15 min to induce the precipitation of proteins and centrifuged at 10,000 rpm for 10 min in a Mikro 220R Hettich centrifuge (Hettich, Tuttlingen, Germany). Supernatants were collected and dried under nitrogen atmosphere using a TurboVap® LV Evaporator (Caliper Life Sciences, Waltham, MA, USA) at 45 °C for 1 h. The dried samples were dispersed with 200 μL methanol, shaken in the multivortex for 5 min and centrifuged. Supernatants were collected, dried again under nitrogen and frozen until the quantification.

Samples were quantified by UHPLC-Q Exactive Orbitrap High-Resolution Mass Spectrometry (Thermo Fisher Scientific, Waltham, MA, USA), using a Thermo Hypersil GOLD column (1.9 μm, 100 × 2.1 mm, Thermo Fisher Scientific, Waltham, MA, USA). The mobile phase was constituted by 0.1% of formic acid in water (mobile phase A) and 0.1% of formic acid in ACN (mobile phase B), at a flow rate of 0.25 mL/min. The gradient conditions are summarized in Table 1. The injection volume was 2 μL, the column temperature 30 °C, and the samples were maintained at 10 °C. A negative ionization mode was used, with the following conditions: sheath gas flow rate: 40 (arbitrary units); auxiliary flow rate: 10 (arbitrary units); sweep gas flow rate: 1 (arbitrary units); spray voltage: 2.5 kV; capillary temperature: 320 °C; S-lens RF level: 55%; aux gas heater temperature: 320 °C.

For the quantification of the quercetin extracted, samples were

Table 1
Gradient conditions used for the quantification of plasma quercetin by UHPLC mass spectrometry. A: 0.1% of formic acid in water; B: 0.1% of formic acid in ACN.

Time (min)	A (%)	B (%)
0	99	1
1	99	1
5	92	8
15	60	40
17	4	96
19	4	96
20	99	1
22	99	1

redissolved in 160 μL of mobile phase (0.1% formic acid in water and 0.1% formic acid in ACN, 50:50 v/v) with 1 μg/mL of sulfadimethoxine, centrifuged at 15,000 rpm for 10 min, and supernatants were injected in the UHPLC. To prepare the calibration curves, standard solutions were prepared in a range from 0.25 to 1 μg/mL of quercetin in methanol. Different volumes of these standards were mixed with 100 μL of commercial rat plasma to form the calibration curve ($R^2 > 0.99$; LOQ: 0.25 μg/mL), and the same extraction procedure was followed.

Finally, pharmacokinetic parameters (T_{max}, C_{max}, $t_{1/2}$, AUC, and MRT) were calculated using the Excel complement PKSolver (Zhang et al., 2010), and the relative oral bioavailability was calculated as the ratio between the areas under the plasma curve for the oral and the intravenous treatment, and expressed in percentage.

2.8. Statistical analysis

For the statistical analysis, Mann-Whitney test was used for the characterization of the nanoparticles. In the case of the analysis of fat accumulation in *C. elegans*, a one-way ANOVA was performed, followed by Tukey's multiple comparison test. For pharmacokinetic analysis, Kruskal-Wallis test was applied, followed by Dunn's multiple comparison test. All tests were done with GrapPad Prism v9.4 (San Diego, CA, USA) and data was plotted using Origin 8.6 (OriginLab, Northampton, USA).

3. Results

3.1. Comparative of empty zein nanoparticles

3.1.1. Physico-chemical and biopharmaceutical characteristics

Zein nanospheres (NS) displayed a mean size of about 230 nm and a negative zeta potential of −41 mV (Table 2). When the wheat germ oil was incorporated in hydroalcoholic solution of zein, the resulting nanocapsules (NC) presented a slightly higher size (close to 250 nm) with a similar negative zeta potential than NS. For both NS and NC, the polydispersity index was always below 0.2, evidencing a high homogeneity of the formulations, and the yield content of the preparative process of the dried powder of nanoparticles was similar (between 61 and 64%).

Fig. 1 shows the morphology and shape of NS and NC. In both cases, nanoparticles presented a spherical shape of about 250 nm. NS were visualized as compact spheres (Fig. 1A), while in the microphotograph of NC (Fig. 1B) it was possible to observe hemispheres characterized by an apparently viscous and sparse nucleus covered by a solid layer of approximately 40 nm.

Fig. 2 shows the FTIR spectra of zein nanoparticles and the different components employed in their preparation (zein, mannitol, and wheat germ oil). Both NS and NC, displayed the characteristic absorption vibrations corresponding to the amide groups of zein: 1653, 1531, and 1238 cm^{-1}, for C = O stretching vibration of amide I, N–H bending coupled to -C-N stretching vibration of amide II, and N–H in plane bending and C-N vibration of amide III, respectively. In addition, the double signal at 3248 and 3190 cm^{-1} corresponded to N–H vibration band, whereas the C-N stretching vibration appeared at 1448 cm^{-1}. Regarding the wheat germ oil, the stretching vibrations associated to

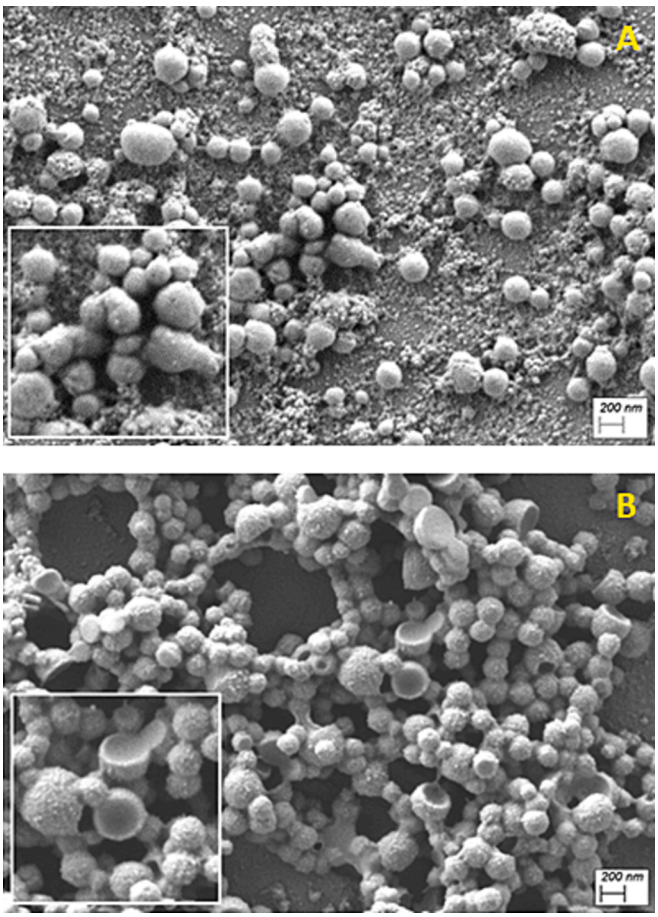

Fig. 1. Scanning electron microscopy (SEM) of zein nanospheres (NS; A) and nanocapsules (NC; B).

$–CH_3$ and $–CH_2$ appeared at 2950–2920 and 2850 cm^{-1}, respectively, whereas the signal observed at 3007 cm^{-1} was attributed to the presence of linoleic acid. One of the most characteristic absorption peaks appeared at 1741 cm^{-1} which is associated to -C = O stretching vibration of fatty acids. It is noticeable that in the IR spectrum of NC, the presence of the oil is detected since a weak intensity signal appears at 1743 cm^{-1} with a shoulder associated at 1726 cm^{-1} that can be attributed to carbonyl group (-C = O) of wheat germ oil interacting with the zein. Finally, mannitol displayed a broad band around 3400 cm^{-1} (OH) and two intense peaks at 1076 and 1016 cm^{-1} corresponding to OH stretching vibrations of alcoholic groups. In the case of the nanoparticles, both showed the two strongest mannitol peaks corresponding to OH stretching vibrations slightly shifted to a higher frequency (1082 and 1022 cm^{-1}).

The surface properties of NS and NC were evaluated by calculating their surface hydrophobicity and their capability to diffuse in pig intestinal mucus by multiple particle tracking (Table 3). Both types of nanocarriers displayed a similar hydrophobicity value. However, the effective diffusion coefficient (<Deff >) was slightly higher for NS than

Table 2
Physico-chemical characteristics of quercetin-loaded nanospheres (Q-NS) and nanocapsules (Q-NC). Data are expressed as mean ± SD (n > 3). PDI: polydispersity index; EE: encapsulation efficiency.

	Size (nm)	PDI	Zeta potential (mV)	Quercetin loading (μg/mg NP)	EE (%)
NS	228 ± 6	0.08 ± 0.05	−40.6 ± 1.6	–	–
NC	247 ± 5	0.11 ± 0.02	−42.1 ± 0.9	–	–
Q-NS	226 ± 2	0.08 ± 0.04	−41.8 ± 4.0	74.8 ± 0.8	82.3 ± 0.5
Q-NC	254 ± 5	0.12 ± 0.01	−44.5 ± 2.1	74.1 ± 7.8	82.3 ± 8.3

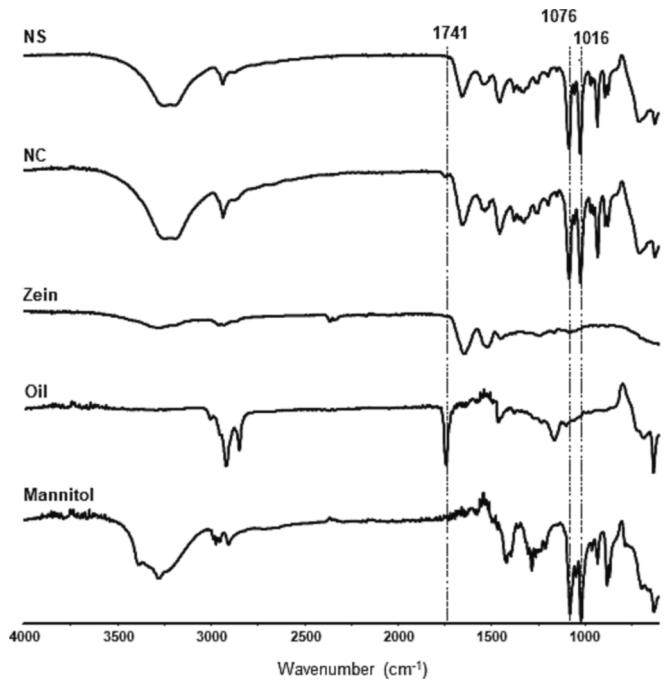

Fig. 2. FTIR spectra of zein nanospheres (NS) and nanocapsules (NC), zein, wheat germ oil, and mannitol. Dashed lines correspond to wheat germ oil (1741 cm^{-1}) and mannitol bands (1076 and 1016 cm^{-1}).

Table 3
Relative hydrophobicity and diffusivity of zein nanoparticles. Data are expressed as mean ± SD (n = 3). For hydrophobicity, values are normalized to the hydrophobicity of NS. < Deff>: Effective Diffusion Coefficient in pig intestinal mucus; D° (water): diffusion coefficient in water; <Deff>/D°: quotient between the diffusion coefficients of nanoparticles in mucus and water (expressed in percentage); R: ratio between < Deff>/D° of NC and the value for NS.

	Relative hydrophobicity	<Deff> · 10^{-9} ($cm^2 \cdot s^{-1}$)	D° (water) · 10^{-9} ($cm^2 \cdot s^{-1}$)	<Deff>/ D° (%)	R
NS	1	0.063 ± 0.036	18.1	0.35 ± 0.12	1.00
NC	0.99	0.046 ± 0.028	18.0	0.26 ± 0.10	0.74

for NC (0.063 and 0.046 × 10^{-9} cm^2/s, respectively). The diffusivity of the nanoparticles in pig intestinal mucus, compared to their ability to move in water, was very low with a value of only 0.35% for NS and 0.26% for NC.

3.1.2. Biodistribution of NS and NC in rat

The biodistribution of NS and NC in the gastrointestinal tract of rats was performed after labelling of nanoparticles with either ^{99m}Tc or Lumogen® Red. The supplementary material section includes images obtained during the biodistribution study with radiolabeled nanoparticles (Fig. 1S), as well as the distribution of an aqueous suspension of Lumogen® red used as a control for comparison purposes (Fig. 2S). In all cases, nanoparticles were dispersed in water and orally administered to animals. Fig. 3 shows the results obtained 4 h post administration. For NS radiolabeled with technetium, radioactivity was mainly visualized in the stomach, small intestine and cecum. On the contrary, the radioactivity associated to NC appeared to be concentrated in the stomach, cecum and ascending colon. Leaving aside the significant presence of radioactivity observed in the stomachs of the animals (associated with the high binding affinity of pertechnetate for the stomach mucosa (Kiratli et al., 2009)), it seemed that NS displayed a longer gastrointestinal residence than NC. This evidence was corroborated when nanoparticles were labelled with Lumogen® Red. In this case, fluorescence associated to NS was mainly observed in the jejunum and ileum of animals forming like a continuous layer in the mucus covering the epithelial surface. On the contrary, for fluorescently labelled NC, no evident signal was observed in the small intestine of animals; although its presence was detected in the cecum of the animals (Fig. 3), confirming their more rapid transit along the gut of animals.

3.2. Comparative of quercetin-loaded zein nanoparticles

3.2.1. Physico-chemical characteristics and in vitro release

Table 2 summarizes the main physico-chemical characteristics of quercetin-loaded nanoparticles. Both formulations, Q-NS and Q-NC, displayed similar mean size, negative zeta potential and PDI values than the non-loaded particles. The quercetin payload was around 75 μg per milligram nanoparticles and the encapsulation efficiency was around 80%.

The *in vitro* release profiles of quercetin (Fig. 4) presented a similar shape for both types of nanoparticles, being capable of releasing a similar amount of quercetin (about 70% of the payload). For both nanoparticles, ca. 30% of the flavonoid content was released after 2 h of incubation in SGF and about an additional 35–40% in the following 4–5 h when they were incubated in SIF. These results suggest that the release of quercetin from the studied zein-based nanoparticles is independent of the pH conditions and the structure of nanoparticles.

3.2.2. In vivo studies in Caenorhabditis elegans

In order to assess the intake of nanoparticles by the nematode *C. elegans*, L4 larvae were put in contact with Lumogen® Red-loaded nanospheres and pictures were taken. Fig. 5A shows the presence of the fluorescent marker encapsulated in nanoparticles all along the gastrointestinal lumen of *C. elegans*, evidencing that nanoparticles enter the worm by the oral route.

In a preliminary study, the effect of free quercetin on the accumulation of fat by *C. elegans* was evaluated. Free quercetin significantly decreased the fat accumulation in *C. elegans* by, at least 5%, compared to the non-treated group of worms ($p < 0.001$). Then, the effect of encapsulated quercetin (at a dose of 50 μM) was analyzed in glucose-supplemented NGM (0.5% (w/v)), using Orlistat as positive control (Fig. 5B). The supplementation with Q-NS significantly decreased the accumulation of fat, ca. 12% ($p < 0.0001$) compared to NGM. This effect was more intense that the effect observed for free quercetin (a 7% more, $p < 0.0001$).

On the contrary, both free zein and empty nanospheres increased the fat content of worms (compared with NGM group). On the other hand, NC supplementation also increased the amount of fat in *C. elegans*, compared with NGM group (ca. 13%; $p < 0.0001$). This effect was similar to that observed when worms were treated with either wheat germ oil or the mixture between zein and the oil. On the contrary, when quercetin was encapsulated (Q-NC), the fat accumulation in the worms was similar to that of control worms (NGM group), demonstrating again the potent effect of quercetin against the accumulation of fat.

3.2.3. Pharmacokinetic assay in rats

For the pharmacokinetic study, Q-NS and Q-NC were orally administered as single oral dose of 15 μg/kg. In all cases, the pharmacokinetic profiles of quercetin presented a similar profile (Fig. 6), characterized by an initial rapid increase of quercetin plasma levels, followed by a plateau up to 8 h post-administration, and finally a slow decrease during the following hours. Overall, the encapsulation of quercetin in nanoparticles increased the amount of the flavonoid quantified in plasma, compared to the oral control formulation.

The pharmacokinetic parameters, calculated from the plasma quercetin levels vs time curve, are summarized in Table 4. For comparisons, the intravenous profile of the quercetin solution in PEG400 and water

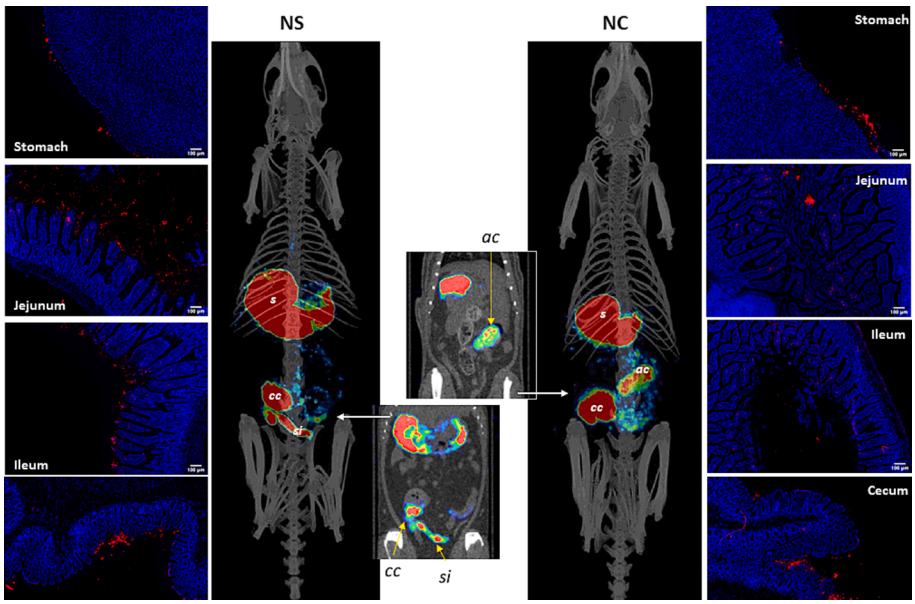

Fig. 3. Biodistribution of NS and NC in the gastrointestinal tract of animals. Images were taken 4 h post-administration. Nanoparticles were either radiolabeled with ^{99m}Tc or fluorescently labelled with Lumogen® Red. Longitudinal slices are also shown. *s*: stomach; *si*: small intestine; *cc*: cecum; *ac*: ascending colon.

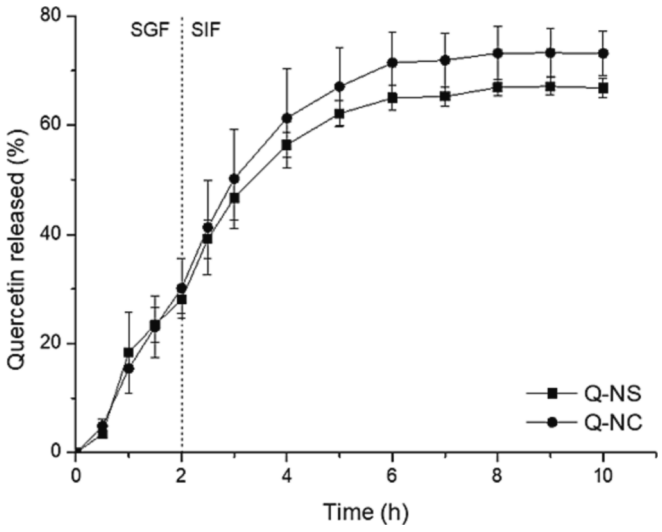

Fig. 4. *In vitro* release profile of quercetin-loaded nanospheres (Q-NS) and quercetin-loaded nanocapsules (Q-NC). Data are expressed as mean ± SD (n = 3).

was employed (data not shown). The quercetin control formulation (Q) displayed the lowest plasma profile, with a C_{max} of 358 ng/mL. On the contrary, Q-NS offered a 6-times higher C_{max} than Q (ca. 1925 ng/mL), whereas, for Q-NC, the C_{max} was found to be three times higher than for the control formulation. In a similar way, the AUC obtained with Q-NC and Q-NS were 5-times and 11-times higher than the control formulation, respectively. Finally, the relative oral bioavailability of quercetin when formulated in zein nanospheres was of about 57%, approximatively two-times higher than when encapsulated in zein nanocapsules (ca. 26%) or>10-fold the value obtained for the conventional control formulation.

4. Discussion

In this work, a comparison between the capability of zein nanospheres and nanocapsules to carry and promote the bioavailability and efficacy of quercetin has been evaluated. The main difference between both types of carriers was that zein nanocapsules included wheat germ oil at an oil-to-zein ratio of 0.1 w/w. In principle, the rationale to include an oil was to increase the payload, to modify the *in vitro* release profile of the loaded flavonoid and to promote quercetin absorption. In this work, and under the experimental conditions tested, zein nanospheres and nanocapsules presented similar physico-chemical characteristics, in terms of size, shape, zeta potential, and surface hydrophobicity (Fig. 1, Table 2 and Table 3). These results were in line with the similar diffusivity calculated for both types of nanocarriers in pig intestinal mucus (Table 3). All of these findings evidenced that the oil, detected by FTIR (Fig. 2), was effectively encapsulated in the nanocapsules. In addition, SEM images show a less robust structure in nanocapsules than in zein nanospheres, coherent with a hollow structure (Fig. 1).

The oral biodistribution in Wistar rats with radiolabeled nanoparticles, NC showed a faster movement along the gastrointestinal tract than NS. In fact, 4 h post-administration, radioactivity associated with NC was observed in the ascending colon, while NS were still in the cecum (Fig. 3). This result would be due to a low capacity of the nanocapsules to interact with the protective mucus layer covering the intestinal epithelium, as it was shown with Lumogen® red labeling. On the contrary, NS displayed a higher ability than NC to interact with intestinal epithelium (Fig. 3). This finding is in agreement with previous reports describing the mucoadhesive behavior of zein nanospheres in vivo (Esposito et al., 2020; Peñalva et al., 2015). This different behavior of NC, compared to NS, could be due to a relative fragility of their structure against enzymatic degradation. Thus, the action of the proteases on the thin wall of nanocapsules would facilitate their degradation and elimination.

It has been described that nanocapsules, compared with nanospheres, can effectively increase drug-loading efficiency, particularly of highly lipophilic compounds (Deng et al., 2020; Raffin Pohlmann et al., 2002). Nevertheless, in our case, both types of nanocarriers displayed similar physico-chemical values with quercetin contents of about 7.5% and entrapment efficiencies of 82% (Table 2). Although the flavonoid payload was in line with previous values reported in the literature (Ersoz et al., 2020; Li et al., 2019; Zhou et al., 2021), nanocapsules did not show a superior capability to load quercetin than nanospheres. On the other hand, both Q-NS and Q-NC displayed similar *in vitro* release kinetics, characterized by a quasi-linear profile (during the first 4 h)

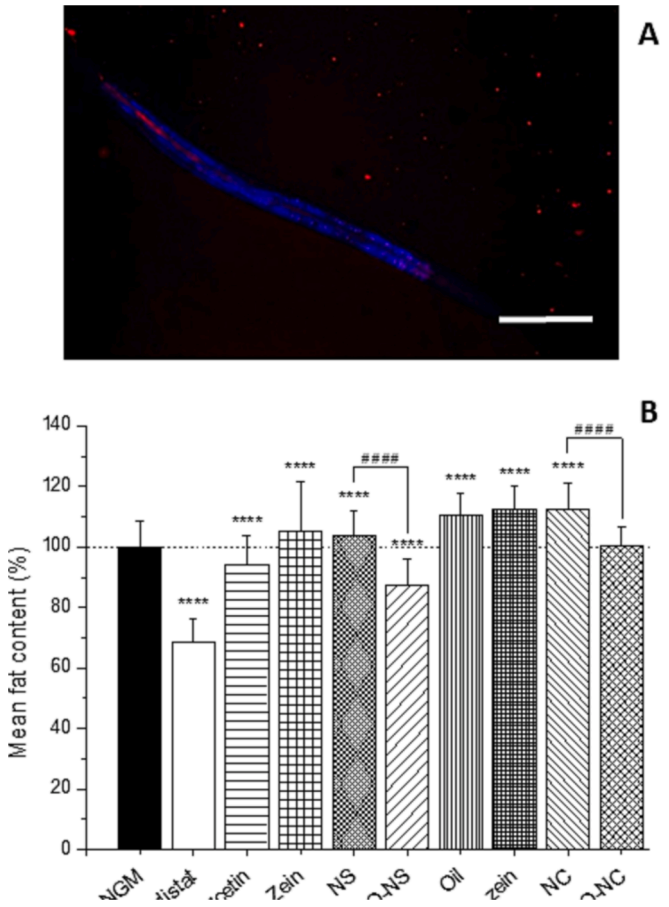

Fig. 5. Evaluation of quercetin formulations in *C. elegans*. (A) Fluorescent image of a worm growth in NGM containing Lumogen® Red-loaded nanospheres. The bar represents 200 μm. (B) Evaluation of the fat accumulation in *C. elegans* cultured on NGM supplemented with glucose (0.5% w/v) and containing the different treatments tested. Data are represented as the mean fat content normalized to control NGM ± SD ($n \geq 92$, ****$p < 0.0001$ compared to NGM; ####$p < 0.0001$). Not all the significances are shown. NS, Q-NS: empty and quercetin-loaded nanospheres; NC, Q-NC: empty and quercetin-loaded nanocapsules. Orlistat was employed as a positive control. Quercetin dose: 50 μM.

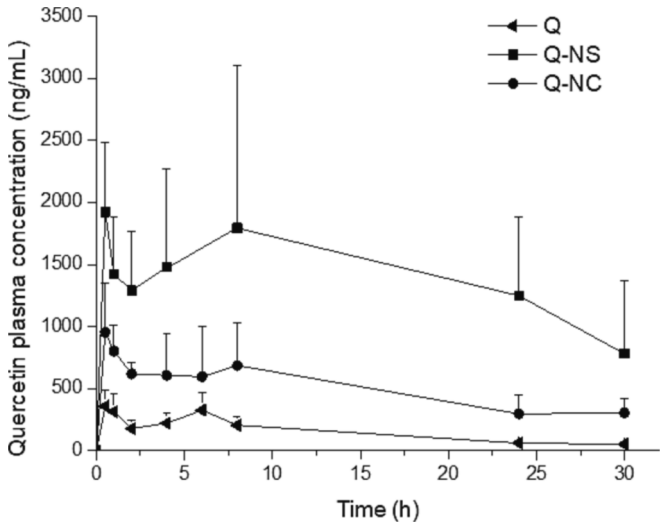

Fig. 6. Pharmacokinetic profile of oral administered free quercetin formulations (free or nanoencapsulated) at a single dose of 15 mg/kg. Data are expressed as mean ± SD ($n \geq 5$). Q: quercetin formulation in an aqueous solution of HP-β-CD; Q-NS: quercetin-loaded nanospheres; Q-NC: quercetin-loaded nanocapsules.

independent of the pH conditions, to later reach a plateau (Fig. 4).

The antihyperlipidemic effect of quercetin was evaluated in *C. elegans* growth in NGM supplemented with glucose (Fig. 5B). Under these experimental conditions, and in agreement with previous results by Lin and co-workers (Lin et al., 2020), quercetin inhibited lipid accumulation in worms. This reducing effect on fat accumulation of quercetin was found to be approximately two-times more intense for nanoencapsulated quercetin (Q-NS) than for the free form. This observation may be explained by a combination of different factors. First, the digestion of zein may generate peptides and hydrolysates with antioxidant activity (Esfandi et al., 2019; Tang and Zhuang, 2014) and, thus, protect quercetin against its oxidative inactivation. Second, the nanoencapsulation of quercetin would offer protection against degradation by *E. coli* (Zhang et al., 2014), used as diet for *C. elegans*. Third, the gut of *C. elegans* is covered by a fuzzy layer of material encasing the microvilli and extending into the intestinal lumen, similar to the mucus layer in the mammals (Everman et al., 2015; Maduro, 2017). The mucoadhesive properties of zein nanoparticles might increase the residence time in close contact with this peritrophic matrix, facilitating quercetin absorption. Comparing with NS, NC significantly increased the storage of lipids in *C. elegans* (Fig. 5B; $p < 0.0001$). This effect can be mainly attributed to the presence of wheat germ oil in the composition of nanocapsules, as empty NC increased significantly fat accumulation (Fig. 5B). Nevertheless, the incorporation of quercetin in nanocapsules (Q-NC) significantly counteracted this deleterious effect, decreasing fat accumulation compared to NC to levels similar to NGM group (Q-NC vs NC, $p < 0.0001$).

Finally, quercetin was orally administered as a single dose of 15 mg/kg to Wistar rats as a conventional aqueous formulation (Q) or loaded in zein-based nanoparticles (Q-NS and Q-NC; Fig. 6). In all cases, the plasma profiles were similar; although higher levels of the flavonoid were observed for the nanoencapsulated quercetin than for the control formulation, particularly for Q-NS. The relative oral bioavailability (Fr) of quercetin in the control formulation (Q) was 5% (Table 4), in agreement with previously published data, ranging from 3.6% to 5.3% (Chen et al., 2005; Li et al., 2021). For nanoencapsulated quercetin, Q-NS displayed the highest relative oral bioavailability (about 57%), two-fold higher than for Q-NC (approx. 26%), evidencing that the former formulation is a better alternative for the formulation of this flavonoid.

This finding seems to be in contradiction with the general idea that nanocapsules (and other types of lipid vesicles) may be an adequate strategy to promote the oral bioavailability of lipophilic compounds, promoting their absorption by the lymphatic system and, at the same time, minimizing its pre-systemic metabolism (Garg et al., 2016; Patel et al., 2019; Pinheiro et al., 2021). In our case, this evident better performance of nanospheres over nanocapsules may be explained by a reduced mechanical strength and a faster transit into the gut (Fig. 3) of the latter. This faster gastrointestinal transit might comparatively difficult the release of quercetin, giving place to a lower relative oral bioavailability. In any case, more experiments would be necessary to confirm this lesser capacity of the nanocapsules and if the phenomenon could be extended to other lipophilic compounds.

In summary, zein-based nanospheres and nanocapsules with similar physico-chemical characteristics can be successfully prepared by desolvation method. Both types of nanoparticles offer a similar capability to encapsulate quercetin, yielding a payload of about 7.5%. Moreover, the nanoencapsulation of quercetin in zein-based nanoparticles improved its efficacy as lowering fat agent in *C. elegans*; although this effect was significantly higher for nanospheres than for nanocapsules, in which the presence of the oil would be deleterious. In a similar way, the nanoencapsulation of quercetin in zein-based nanoparticles improved the relative oral bioavailability of this flavonoid. Nevertheless, again,

Table 4
Pharmacokinetic parameters obtained for the administration of free and nanoencapsulated quercetin at 15 mg/kg. Data are expressed as mean ± SD ($n \geq 5$, *$p < 0.05$, **$p < 0.01$, nanoparticles compared to Q). i.v.: intravenous administration of quercetin; Q: quercetin formulation in an aqueous solution of HP-β-CD; Q-NS: quercetin-loaded nanospheres; Q-NC: quercetin-loaded nanocapsules. T_{max}: time to reach maximum plasma concentration; C_{max}: maximum plasma concentration; $t_{1/2}$: half-life; MRT: mean residence time; AUC: area under the curve; Fr: relative oral bioavailability.

	T_{max} (h)	C_{max} (ng/mL)	$t_{1/2}$ (h)	MRT (h)	AUC $_{0-\infty}$ (ng h/mL)	Fr (%)
i.v.	0	69494 ± 13067	4.0 ± 2.1	3.5 ± 2.0	97524 ± 34067	100
Q	0.5	358 ± 128	8.2 ± 1.7	12.3 ± 2.3	4790 ± 1478	4.9
Q-NS	0.5	1925 ± 561**	11.5 ± 4.2	16.7 ± 6.4	56019 ± 44131**	57.4
Q-NC	0.5	955 ± 400	20.1 ± 4.8**	30.5 ± 7.1**	24986 ± 8860*	25.6

nanospheres showed better performance than nanocapsules.

CRediT authorship contribution statement

Raquel Campión: Conceptualization, Methodology, Data curation, Investigation, Software, Visualization, Formal analysis, Writing – original draft. **Carlos J. Gonzalez-Navarro:** Conceptualization, Resources, Writing – review & editing, Funding acquisition, Supervision. **Ana Luisa Martínez López:** Conceptualization, Methodology, Data curation, Investigation, Software, Visualization, Formal analysis. **M. Cristina Martínez-Oharriz:** Methodology, Data curation, Software, Writing – review & editing. **Cristina Matías:** Methodology, Resources, Data curation. **María-José Sáiz-Abajo:** Methodology, Resources, Data curation, Writing – review & editing. **Maria Collantes:** Methodology, Formal analysis, Writing – review & editing. **Ivan Peñuelas:** Conceptualization, Resources, Funding acquisition, Supervision. **Juan M. Irache:** Conceptualization, Resources, Writing – review & editing, Funding acquisition, Supervision.

Declaration of Competing Interest

The authors declare that they have no known competing financial interests or personal relationships that could have appeared to influence the work reported in this paper.

Data availability

Data will be made available on request.

Acknowledgements

This work was partially funded by the Government of Navarra (PC127-128 METANOB). The authors thank the Caenorhabditis Genetics Center (CGC), which is funded by NIH Office of Research Infrastructure Programs (P40 OD010440), for providing *C. elegans* and *E. coli* strains.

Appendix A. Supplementary material

Supplementary data to this article can be found online at https://doi.org/10.1016/j.ijpharm.2023.123216.

References

Abdel-Raouf, N., Ibraheem, I.B.M., Abdel-Tawab, S., Naser, Y.A.G., 2011. Antimicrobial and antihyperlipidemic activities of isolated quercetin from *Anabaena Aequalis*. J. Phycol. 47, 955–962. https://doi.org/10.1111/j.1529-8817.2011.01020.x.

Abdulkarim, M., Agulló, N., Cattoz, B., Griffiths, P., Bernkop-Schnürch, A., Gómez Borros, S., Gumbleton, M., 2015. Nanoparticle diffusion within intestinal mucus: Three-dimensional response analysis dissecting the impact of particle surface charge, size and heterogeneity across polyelectrolyte, pegylated and viral particles. Eur. J. Pharm. Biopharm. 97, 230–238. https://doi.org/10.1016/j.ejpb.2015.01.023.

Amidon, S., Brown, J.E., Dave, V.S., 2015. Colon-Targeted Oral Drug Delivery Systems: Design Trends and Approaches. AAPS PharmSciTech 16, 731–741. https://doi.org/10.1208/s12249-015-0350-9.

Aranaz, P., Navarro-Herrera, D., Zabala, M., Romo-Hualde, A., López-Yoldi, M., Vizmanos, J.L., Milagro, F.I., González-Navarro, C.J., 2020. Phenolic compounds reduce the fat content in *Caenorhabditis elegans* by affecting lipogenesis, lipolysis, and different stress responses. Pharmaceuticals 13, 1–33. https://doi.org/10.3390/ph13110355.

Barbosa, A.I., Costa Lima, S.A., Reis, S., 2019. Application of pH-responsive fucoidan/chitosan nanoparticles to improve oral quercetin delivery. Molecules 24. https://doi.org/10.3390/molecules24020346.

Başaran, E., Öztürk, A.A., Şenel, B., Demirel, M., Sarica, Ş., 2022. Quercetin, Rutin And Quercetin-Rutin Incorporated Hydroxypropyl β-Cyclodextrin Inclusion Complexes. Eur. J. Pharm. Sci. 172, 106153 https://doi.org/10.1016/j.ejps.2022.106153.

Bouman, J., Belton, P., Venema, P., van der Linden, E., de Vries, R., Qi, S., 2015. The Development of Direct Extrusion-Injection Moulded Zein Matrices as Novel Oral Controlled Drug Delivery Systems. Pharm. Res. 32, 2775–2786. https://doi.org/10.1007/s11095-015-1663-9.

Braun, J.B.S., Ruchel, J.B., Adefegha, S.A., Coelho, A.P.V., Trelles, K.B., Signor, C., Rubin, M.A., Oliveira, J.S., Dornelles, G.L., de Andrade, C.M., Castilhos, L.G., Leal, D. B.R., 2017. Neuroprotective effects of pretreatment with quercetin as assessed by acetylcholinesterase assay and behavioral testing in poloxamer-407 induced hyperlipidemic rats. Biomed. Pharmacother. 88, 1054–1063. https://doi.org/10.1016/j.biopha.2017.01.134.

Chen, X., Yin, O.Q.P., Zuo, Z., Chow, M.S.S., 2005. Pharmacokinetics and modeling of quercetin and metabolites. Pharm. Res. https://doi.org/10.1007/s11095-005-4584-1.

Deng, S., Gigliobianco, M.R., Censi, R., Di Martino, P., 2020. Polymeric Nanocapsules as Nanotechnological Alternative for Drug Delivery System: Current Status. Challenges and Opportunities. Nanomaterials 10, 847. https://doi.org/10.3390/nano10050847.

Dhanya, R., 2022. Quercetin for managing type 2 diabetes and its complications, an insight into multitarget therapy. Biomed. Pharmacother. 146, 112560 https://doi.org/10.1016/j.biopha.2021.112560.

Ersoz, M., Erdemir, A., Derman, S., Arasoglu, T., Mansuroglu, B., 2020. Quercetin-loaded nanoparticles enhance cytotoxicity and antioxidant activity on C6 glioma cells. Pharm. Dev. Technol. 25, 757–766. https://doi.org/10.1080/10837450.2020.1740933.

Esfandi, R., Walters, M.E., Tsopmo, A., 2019. Antioxidant properties and potential mechanisms of hydrolyzed proteins and peptides from cereals. Heliyon 5, e01538.

Esposito, D., Conte, C., D'Angelo, I., Miro, A., Ungaro, F., Quaglia, F., 2020. Mucoadhesive zein/beta-cyclodextrin nanoparticles for the buccal delivery of curcumin. Int. J. Pharm. 586, 119587 https://doi.org/10.1016/j.ijpharm.2020.119587.

Everman, J.L., Ziaie, N.R., Bechler, J., Bermudez, L.E., 2015. Establishing *Caenorhabditis elegans* as a model for Mycobacterium avium subspecies hominissuis infection and intestinal colonization. Biol. Open 4, 1330–1335. https://doi.org/10.1242/bio.012260.

Garg, B., Katare, O.P., Beg, S., Lohan, S., Singh, B., 2016. Systematic development of solid self-nanoemulsifying oily formulations (S-SNEOFs) for enhancing the oral bioavailability and intestinal lymphatic uptake of lopinavir. Colloids Surfaces B Biointerfaces 141, 611–622. https://doi.org/10.1016/j.colsurfb.2016.02.012.

Inchaurraga, L., Martín-Arbella, N., Zabaleta, V., Quincoces, G., Peñuelas, I., Irache, J.M., 2015. *In vivo* study of the mucus-permeating properties of PEG-coated nanoparticles following oral administration. Eur. J. Pharm. Biopharm. 97, 280–289. https://doi.org/10.1016/j.ejpb.2014.12.021.

Kaletta, T., Hengartner, M.O., 2006. Finding function in novel targets: *C. elegans* as a model organism. Nat. Rev. Drug Discov. 5, 387–399. https://doi.org/10.1038/nrd2031.

Kandemir, K., Tomas, M., McClements, D.J., Capanoglu, E., 2022. Recent advances on the improvement of quercetin bioavailability. Trends Food Sci. Technol. 119, 192–200. https://doi.org/10.1016/j.tifs.2021.11.032.

Kiratli, P.O., Aksoy, T., Bozkurt, M.F., Orhan, D., 2009. Detection of ectopic gastric mucosa using ^{99m}Tc pertechnetate: Review of the literature. Ann. Nucl. Med. 23, 97–105. https://doi.org/10.1007/s12149-008-0204-6.

Li, H., Wang, D., Liu, C., Zhu, J., Fan, M., Sun, X., Wang, T., Xu, Y., Cao, Y., 2019. Fabrication of stable zein nanoparticles coated with soluble soybean polysaccharide for encapsulation of quercetin. Food Hydrocoll. 87, 342–351. https://doi.org/10.1016/j.foodhyd.2018.08.002.

Li, H., Li, M., Fu, J., Ao, H., Wang, W., Wang, X., 2021. Enhancement of oral bioavailability of quercetin by metabolic inhibitory nanosuspensions compared to conventional nanosuspensions. Drug Deliv. 28, 1226–1236. https://doi.org/10.1080/10717544.2021.1927244.

Li, Y., Yao, J., Han, C., Yang, J., Chaudhry, M.T., Wang, S., Liu, H., Yin, Y., 2016. Quercetin, inflammation and immunity. Nutrients 8, 1–14. https://doi.org/10.3390/nu8030167.

Lin, Y., Yang, N., Bao, B., Wang, L., Chen, J., Liu, J., 2020. Luteolin reduces fat storage in *Caenorhabditis elegans* by promoting the central serotonin pathway. Food Funct. 11, 730–740. https://doi.org/10.1039/C9FO02095K.

Lu, Z., Bu, C., Hu, W., Zhang, H., Liu, M., Lu, M., Zhai, G., 2018. Preparation and *in vitro* and *in vivo* evaluation of quercetin-loaded mixed micelles for oral delivery. Biosci. Biotechnol. Biochem. 82, 238–246. https://doi.org/10.1080/09168451.2017.1419852.

Luca, S.V., Macovei, I., Bujor, A., Miron, A., Skalicka-Woźniak, K., Aprotosoaie, A.C., Trifan, A., 2020. Bioactivity of dietary polyphenols: The role of metabolites. Crit. Rev. Food Sci. Nutr. 60, 626–659. https://doi.org/10.1080/10408398.2018.1546669.

Maduro, M.F., 2017. Gut development in *C. elegans*. Semin. Cell Dev. Biol. 66, 3–11. https://doi.org/10.1016/j.semcdb.2017.01.001.

Mahadev, M., Nandini, H.S., Ramu, R., Gowda, D.V., Almarhoon, Z.M., Al-Ghorbani, M., Mabkhot, Y.N., 2022. Fabrication and Evaluation of Quercetin Nanoemulsion: A Delivery System with Improved Bioavailability and Therapeutic Efficacy in Diabetes Mellitus. Pharmaceuticals 15, 70. https://doi.org/10.3390/ph15010070.

Martínez-López, A.L., Pangua, C., Reboredo, C., Campión, R., Morales-Gracia, J., Irache, J.M., 2020. Protein-based nanoparticles for drug delivery purposes. Int. J. Pharm. 581, 119289 https://doi.org/10.1016/j.ijpharm.2020.119289.

Martínez-López, A.L., González-Navarro, C.J., Aranaz, P., Vizmanos, J.L., Irache, J.M., 2021. *In vivo* testing of mucus-permeating nanoparticles for oral insulin delivery using *Caenorhabditis elegans* as a model under hyperglycemic conditions. Acta Pharm. Sin. B 11, 989–1002. https://doi.org/10.1016/j.apsb.2021.02.020.

Mazza, A., Nicoletti, M., Lenti, S., Torin, G., Rigatelli, G., Fratter, A., Pellizzato, M., 2021. Effectiveness and safety of nutraceutical compounds added to ezetimibe treatment in hypertensive and hyper-cholesterolemic subjects with statin-intolerance. J. Hypertens. 39, e371.

Moreno, L.C.G. e I., Puerta, E., Suárez-Santiago, J.E., Santos-Magalhães, N.S., Ramirez, M.J., Irache, J.M., 2017. Effect of the oral administration of nanoencapsulated quercetin on a mouse model of Alzheimer's disease. Int. J. Pharm. 517, 50–57. 10.1016/j.ijpharm.2016.11.061.

Mzhel'skaya, K. V., Trusov, N. V., Guseva, G.N., Aksenov, I. V., Kravchenko, L. V., Tutelyan, V.A., 2019. Effects of Quercetin on Expression of Genes of Carbohydrate and Lipid Metabolism Enzymes in the Liver of Rats Receiving High-Fructose Ration. Bull. Exp. Biol. Med. 167, 263–266. 10.1007/s10517-019-04505-0.

Nabavi, S.F., Russo, G.L., Daglia, M., Nabavi, S.M., 2015. Role of quercetin as an alternative for obesity treatment: You are what you eat! Food Chem. 179, 305–310. https://doi.org/10.1016/j.foodchem.2015.02.006.

Navarro-Herrera, D., Aranaz, P., Eder-Azanza, L., Zabala, M., Hurtado, C., Romo-Hualde, A., Martínez, J.A., González-Navarro, C.J., Vizmanos, J.L., 2018. Dihomo-gamma-linolenic acid induces fat loss in: *C. Elegans* in an omega-3-independent manner by promoting peroxisomal fatty acid β-oxidation. Food Funct. 9, 1621–1637. 10.1039/c7fo01625e.

Nekohashi, M., Ogawa, M., Ogihara, T., Nakazawa, K., Kato, H., Misaka, T., Abe, K., Kobayashi, S., 2014. Luteolin and Quercetin Affect the Cholesterol Absorption Mediated by Epithelial Cholesterol Transporter Niemann-Pick C1-Like 1 in Caco-2 Cells and Rats. PLoS One 9, e97901.

Nishimura, M., Muro, T., Kobori, M., Nishihira, J., 2019. Effect of Daily Ingestion of Quercetin-Rich Onion Powder for 12 Weeks on Visceral Fat: A Randomised, Double-Blind, Placebo-Controlled. Parallel-Group Study. Nutrients 12, 91. https://doi.org/10.3390/nu12010091.

Patel, M., Mundada, V., Sawant, K., 2019. Enhanced intestinal absorption of asenapine maleate by fabricating solid lipid nanoparticles using TPGS: elucidation of transport mechanism, permeability across Caco-2 cell line and in vivo pharmacokinetic studies. Artif. Cells, Nanomedicine, Biotechnol. 47, 144–153. https://doi.org/10.1080/21691401.2018.1546186.

Peñalva, R., Esparza, I., González-Navarro, C.J., Quincoces, G., Peñuelas, I., Irache, J.M., 2015. Zein nanoparticles for oral folic acid delivery. J. Drug Deliv. Sci. Technol. 30, 450–457. https://doi.org/10.1016/j.jddst.2015.06.012.

Peñalva, R., Esparza, I., Morales-Gracia, J., González-Navarro, C.J., Larrañeta, E., Irache, J.M., 2019. Casein nanoparticles in combination with 2-hydroxypropyl-β-cyclodextrin improves the oral bioavailability of quercetin. Int. J. Pharm. 570, 118652 https://doi.org/10.1016/j.ijpharm.2019.118652.

Penalva, R., González-Navarro, C.J., Gamazo, C., Esparza, I., Irache, J.M., 2017. Zein nanoparticles for oral delivery of quercetin: Pharmacokinetic studies and preventive anti-inflammatory effects in a mouse model of endotoxemia. Nanomedicine Nanotechnology. Biol. Med. 13, 103–110. https://doi.org/10.1016/j.nano.2016.08.033.

Pinheiro, R.G.R., Pinheiro, M., Neves, A.R., 2021. Nanotechnology innovations to enhance the therapeutic efficacy of quercetin. Nanomaterials 11, 1–26. https://doi.org/10.3390/nano11102658.

Raffin Pohlmann, A., Weiss, V., Mertins, O., Pesce da Silveira, N., Stanisçuaski Guterres, S., 2002. Spray-dried indomethacin-loaded polyester nanocapsules and nanospheres: development, stability evaluation and nanostructure models. Eur. J. Pharm. Sci. 16, 305–312. https://doi.org/10.1016/S0928-0987(02)00127-6.

Reboredo, C., González-Navarro, C.J., Martínez-Oharriz, C., Martínez-López, A.L., Irache, J.M., 2021. Preparation and evaluation of PEG-coated zein nanoparticles for oral drug delivery purposes. Int. J. Pharm. 597, 120287 https://doi.org/10.1016/j.ijpharm.2021.120287.

Serban, M., Sahebkar, A., Zanchetti, A., Mikhailidis, D.P., Howard, G., Antal, D., Andrica, F., Ahmed, A., Aronow, W.S., Muntner, P., Lip, G.Y.H., Graham, I., Wong, N., Rysz, J., Banach, M., 2016. Effects of Quercetin on Blood Pressure: A Systematic Review and Meta-Analysis of Randomized Controlled Trials. J. Am. Heart Assoc. 5, e002713.

Shao, Y., Yu, Y., Li, C., Yu, J., Zong, R., Pei, C., 2016. Synergistic effect of quercetin and 6-gingerol treatment in streptozotocin induced type 2 diabetic rats and poloxamer P-407 induced hyperlipidemia. RSC Adv. 6, 12235–12242. https://doi.org/10.1039/C5RA16493A.

Tang, N., Zhuang, H., 2014. Evaluation of antioxidant activities of zein protein fractions. J. Food Sci. 79, C2174–C2184. https://doi.org/10.1111/1750-3841.12686.

Tran, T.H., Guo, Y., Song, D., Bruno, R.S., Lu, X., 2014. Quercetin-Containing Self-Nanoemulsifying Drug Delivery System for Improving Oral Bioavailability. J. Pharm. Sci. 103, 840–852. https://doi.org/10.1002/jps.23858.

Vogiatzoglou, A., Mulligan, A.A., Lentjes, M.A.H., Luben, R.N., Spencer, J.P.E., Schroeter, H., Khaw, K.-T., Kuhnle, G.G.C., 2015. Flavonoid Intake in European Adults (18 to 64 Years). PLoS One 10, e0128132.

Winters, E.P., Deardorff, D.L., 1958. Zein as a Film-Type Coating for Medicinal Tablets. J. Am. Pharm. Assoc. 47, 608–612. https://doi.org/10.1002/jps.3030470823.

Yang, Z., McClements, D.J., Peng, X., Qiu, C., Long, J., Zhao, J., Xu, Z., Meng, M., Chen, L., Jin, Z., 2022. Co-encapsulation of quercetin and resveratrol in zein/carboxymethyl cellulose nanoparticles: characterization, stability and *in vitro* digestion. Food Funct. 13, 11652–11663. https://doi.org/10.1039/D2FO02718F.

Yang, H., Yang, T., Heng, C., Zhou, Y., Jiang, Z., Qian, X., Du, L., Mao, S., Yin, X., Lu, Q., 2019. Quercetin improves nonalcoholic fatty liver by ameliorating inflammation, oxidative stress, and lipid metabolism in db / db mice. Phyther. Res. 33, 3140–3152. https://doi.org/10.1002/ptr.6486.

Yin, H., Lu, T., Liu, L., Lu, C., 2015. Preparation, characterization and application of a novel biodegradable macromolecule: Carboxymethyl zein. Int. J. Biol. Macromol. 72, 480–486. https://doi.org/10.1016/j.ijbiomac.2014.08.025.

Zhang, Y., Huo, M., Zhou, J., Xie, S., 2010. PKSolver: An add-in program for pharmacokinetic and pharmacodynamic data analysis in Microsoft Excel. Comput. Methods Programs Biomed. 99, 306–314. https://doi.org/10.1016/j.cmpb.2010.01.007.

Zhang, Z., Peng, X., Li, S., Zhang, N., Wang, Y., Wei, H., 2014. Isolation and Identification of Quercetin Degrading Bacteria from Human Fecal Microbes. PLoS One 9, e90531.

Zhou, J.F., Zheng, G.D., Wang, W.J., Yin, Z.P., Chen, J.G., Li, J.E., Zhang, Q.F., 2021. Physicochemical properties and bioavailability comparison of two quercetin loading zein nanoparticles with outer shell of caseinate and chitosan. Food Hydrocoll. 120, 106959 https://doi.org/10.1016/j.foodhyd.2021.106959.

Zhu, G., Yin, F., Wang, L., Wei, W., Jiang, L., Qin, J., 2016. Modeling type 2 diabetes-like hyperglycemia in *C. elegans* on a microdevice. Integr. Biol. (United Kingdom) 8, 30–38. https://doi.org/10.1039/c5ib00243e.